Non-neutral plasma equilibria, trapping, separatrices, and separatrix crossing in magnetic mirrors

J. Fajans[a)]
Department of Physics, University of California, Berkeley, California 94720

(Received 20 December 2002; accepted 28 January 2003)

The equilibria of non-neutral plasmas confined in Penning–Malmberg traps with axial varying (mirror) magnetic fields exhibit numerous unusual features, including potential differences along field lines, plasma density variations, trapped particles in both the high and low field regions, and unusual separatrices between trapped and untrapped particles. Mirror fields play prominent roles in a number of recent experiments, and overly simplistic models of the equilibria can lead to errors in the interpretation of experimental results. © *2003 American Institute of Physics.*
[DOI: 10.1063/1.1564820]

I. INTRODUCTION

Many experiments have confined non-neutral plasmas in Penning–Malmberg traps. Typically, radial confinement in these traps is provided by a uniform axial magnetic field. Recently, the effects of variations in the axial magnetic fields have come under scrutiny. Effects of such ''mirror'' fields come into play when transporting trapped plasmas from one trap to another, as is common in anti-matter traps. Moreover, researchers have speculated that inadvertent mirror fields are responsible for transport in Penning–Malmberg traps.[1,2]

The equilibrium properties of non-neutral plasmas in uniform magnetic fields were identified long ago,[3,4] and mirror fields in neutral plasmas were extensively studied in the fusion community. However there has been little published work on the equilibria of non-neutral plasmas in magnetic mirrors. Davidson *et al.*[5] considered a rather different geometry than the Penning–Malmberg trap: An annular electron layer surrounded by a conducting wall and confined in a magnetic mirror. Dubin and O'Neil developed a general framework that encompasses global thermal equilibrium plasmas in mirror fields, but did not analyze the mirror states closely.[6] Gopalan and Fajans discussed the mirror equilibria in Penning–Malmberg traps in several conference papers[7,8] and in Gopalan's Ph.D. thesis.[9] Here I report some of these last results, some new analytic results, and descriptions of the velocity-space separatrix crossings.

The analysis leads to several surprising conclusions:

(1) When the plasma is dense and cold, the plasma density is roughly proportional to the magnetic field. However, when the plasma is hot or tenuous, the density becomes independent of the magnetic field.
(2) Inside the plasma, the electrostatic potential is not constant along the magnetic-field lines; a potential arises which attracts particles into the high field region along most, but not all, of the field lines.
(3) In the high field region the plasma is ''thinner'' than what one would expect from following the field lines.
(4) Different classes of particles are trapped in *both* the low and the high field region:
   (a) The velocity-space separatrix bounding the trapped and untrapped populations in the low field region is significantly modified from the standard mirror field separatrix (see Fig. 1).
   (b) The velocity-space separatrix bounding the trapped and untrapped populations in the high field region has no analog in the standard mirror field analysis.

For simplicity, I will model a pure-electron plasma stored in two uniform magnetic-field regions B_L and B_H, and ignore the transition region in between (see Fig. 2). (The transition region must be long enough that the magnetic moment of the electrons is adiabatically conserved, and that electrons follow the magnetic-field lines.) The results can be easily extended to continually varying fields. As with all Penning–Malmberg traps, the plasma is ultimately confined axially by external electrostatic fields applied to the plasma ends.

Throughout the paper I assume that the plasma electrons are in thermal equilibrium along individual field lines, though not necessarily in global thermal equilibrium. The equilibrium is particularly simple for very cold, flat-top plasmas, and I analyze this case first. Then the analysis is extended to finite-temperature, flat-top plasmas, which exhibit all the significant features of the equilibrium. Plasmas with arbitrary profiles, and plasmas in global thermal equilibrium are analyzed next. Then I discuss trapped particles and separatrices. The main part of the paper concludes by examining separatrix crossing in these equilibria, and its implications for the work in Ref. 2. Finally, the Appendices give two derivations not presented earlier. This paper presents only theoretical results; there is good experimental evidence for some of the results presented here, including conclusions 1 and 3 above, in Gopalan's Ph.D. thesis.[9]

II. EQUILIBRIA

Typically, thermal equilibrium along field lines is established after only a few plasma oscillations. The plasma density then obeys Boltzmann's relation

$$n_H(r_H) = n_L(r_L)\exp\left(\frac{e\Delta\phi(r_L)}{kT}\right). \tag{1}$$

a)Electronic mail: joel@physics.berkeley.edu

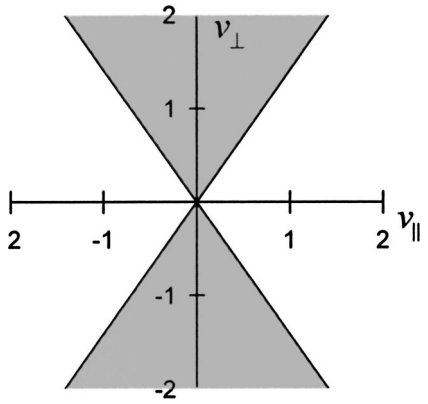

FIG. 1. The "standard" separatrix between trapped (shaded) and untrapped noninteracting particles for the case $\beta=0.5$, where β is the mirror ratio B_H/B_L-1. The parallel $v_\parallel$ and perpendicular $v_\perp$ temperatures are normalized to the thermal temperature.

Here $n_H(r_H)$ is the density at radius r_H in the high field region, $n_L(r_L)$ is the density at radius r_L in the low field region, e is the electron charge, and kT is the electron thermal energy. The temperature T is assumed constant throughout the plasma. The high field radius r_H is linked to the low field radius r_L by the magnetic field lines: $r_H=r_L/\sqrt{1+\beta}$, where β is the magnetic field increase defined by $B_H=(1+\beta)B_L$. The potential $\Delta\phi(r_L)$ is the difference in potential along the field line that begins at r_L and goes to r_H. Note that $\Delta\phi(r_L)$ does not go to zero at the wall, as it is the difference between potential at $r_L=R_w$ in the low field region, and the potential at the linked radius r_H, less than R_w for $\beta>0$, in the high field region.

A. Zero temperature equilibria

In the limit $T\to 0$, the potential must be constant along all field lines inside the plasma. If it is not, then the Boltzmann relation [Eq. (1)] predicts that there will be enormous density changes along the field lines. This does not mean, however, that the density itself be constant along a field line. Because field lines converge in high field region, the only way to make the potential constant along field lines is for the plasma density to be proportional to magnetic field. (In contrast, the density would be constant along the field lines in a neutral plasma. The compression caused by the converging field lines is exactly cancelled by reflections from the increasing magnetic field.)

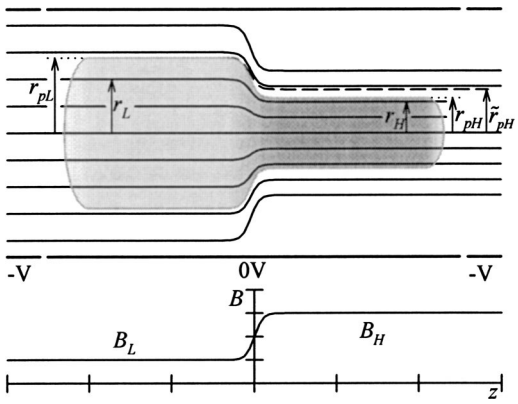

FIG. 2. Typical magnetic field, magnetic field lines, and plasma profile in a stepped magnetic field. For clarity, the difference between $\tilde{r}_{pH}$ and r_{pH} has been exaggerated.

Thus, the zero temperature, flat-top equilibrium consists of two columns of constant, but different density, related by $n_H=n_L(1+\beta)$. The on-axis($r=0$) potentials of the two columns must match. If the two columns had outer radii r_p linked together along a field line, the on-axis high magnetic-field potential would be too negative by a factor proportional to $\ln(1+\beta)$. Consequently the radius of the high density column, r_{pH}, must be smaller than the linked radius of the low density column, $\tilde{r}_{pH}=r_{pL}/\sqrt{1+\beta}$. For small β, the discrepancy $1-r_{pH}/\tilde{r}_{pH}\approx\beta/[4\ln(R_w/r_{pL})]$ is small.

The $T\to 0$ equilibria can be easily extended to arbitrary radial profiles by requiring that the density along linked radii increase by $1+\beta$. The potential along field lines will still be constant inside the plasma, and the high field plasma radius will be somewhat smaller than the low field linked radius.

B. Flat-top, finite temperature equilibria

While a flat-top, finite temperature plasma is somewhat unphysical, such plasmas exhibit all the essential features of the mirror equilibria and are analytically tractable. A straightforward calculation (see Appendix A) employing the Boltzmann and Poisson equations shows that, in the limit of small β, the potential difference across linked field lines inside the plasma is given by

$$\Delta\phi(r_L)=\beta\frac{kT}{e}[1-A\mathrm{I}_0(r_L/\lambda_{dL})], \tag{2}$$

where λ_{dL} is the on-axis Debye length in the low field region, I_0 and I_1 are modified Bessel functions, and

$$A=\frac{\lambda_{dL}^2+r_{pL}^2/4}{\lambda_{dL}[\lambda_{dL}\mathrm{I}_0(r_{pL}/\lambda_{dL})+r_{pL}\mathrm{I}_1(r_{pL}/\lambda_{dL})\ln(R_w/r_{pL})]}. \tag{3}$$

A typical example is shown in Fig. 3.

When $r_{pL}\gg\lambda_{dL}$ (or, equivalently, $r_{pH}\gg\lambda_{dH}$), $A\to\sqrt{2\pi r_{pL}^3/\lambda_d^3}\exp(-r_{pL}/\lambda_d)/\ln(R_w/r_{pL})$ is small, and the on-axis potential difference increases by approximately $\beta kT/e$ in the high field region. As expected, the central density increases by approximately $1+\beta$. A gets larger as λ_{dL} approaches r_{pL}, and the on-axis potential difference gets smaller, eventually approaching zero when $\lambda_{dL}\gtrsim r_{pL}$. Here the density barely increases in the high field region, as the plasma essentially behaves like a gas of noninteracting particles.

Off the axis ($r>0$,) the potential difference diminishes. At the cut-off radius r_{cL}, defined by $1=A\mathrm{I}_0(r_{cL}/\lambda_{dL})$, the potential difference changes sign. For greater radii the density in the low field region is higher than the density at the linked radius in the high field region. This has the necessary effect of "cutting" the high-field plasma off at some radius between $r_{cL}/\sqrt{1+\beta}$ and $\tilde{r}_{pH}$. Note that r_{cL} is independent of β.

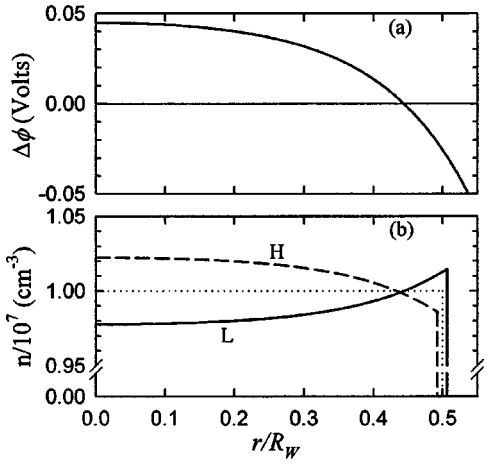

FIG. 3. (a) The potential difference along linked field lines, for an initially flat-top plasma. Before the application of the magnetic field gradient of $\beta=0.05$, the normalized plasma radius was $r_{p0}/R_w=0.5$, with wall radius $R_w=2$ cm. The plasma temperature was $T=1$ eV, and the resulting densities in the low and high field regions are shown by the solid and dashed lines in (b). For these parameters, $A=0.107$.

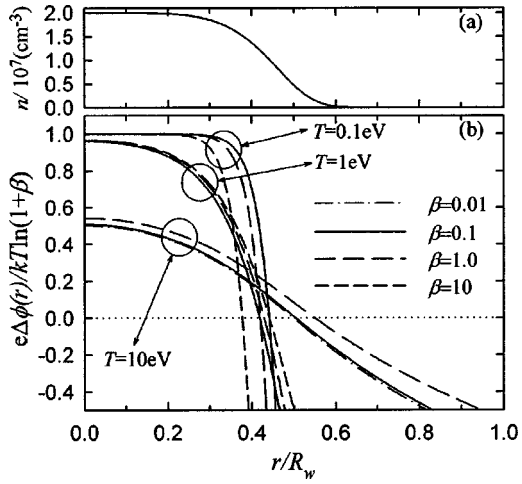

FIG. 5. A survey of the normalized potential difference (b) for the density profile (a). [The profile shown in (a) is the profile obtained at $\beta=0$.] For $\beta=0$, the Debye length λ_d/R_w is about 0.027 at $T=0.1$ eV, 0.085 at $T=1$ eV, and 0.27 at $T=10$ eV. Thus, only at the hottest temperature is the plasma radius comparable to the Debye length, and does the potential difference at the origin deviate significantly from $kT\ln(1+\beta)/e$.

C. Local and global thermal equilibria

While no analytic solution exists for finite temperature, general radial density profiles, it is easy to find the equilibria numerically by iteratively solving the Boltzmann and Poisson equations. A typical solution is shown in Fig. 4. The wide-ranging parameter scan shown in Fig. 5 demonstrates that all equilibria roughly resemble the one shown in Fig. 4.

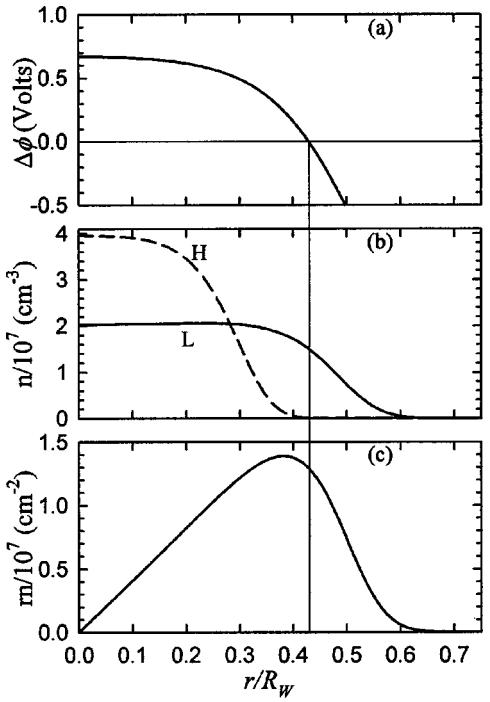

FIG. 4. (a) The potential difference along linked field lines, for a realistic profile plasma, in a magnetic field gradient of $\beta=1.0$. The plasma temperature was $T=1$ eV, the wall radius of $R_w=2$ cm, and the resulting densities in the low and high field regions are shown by the solid and dashed lines in (b). In (c), the low field density profile is multiplied by the weighting factor r, showing that most of the plasma is in the positive $\Delta\phi$ region.

However, there a few trends: (1) For cold, dense plasmas, $e\Delta\phi \lesssim kT\ln(1+\beta)$, and the high field density increases proportional to $1+\beta$. For very hot or tenuous plasmas ($\lambda_d \gtrsim r_p$), the potential difference is much smaller than $kT\ln(1+\beta)$, and the density increases less than linearly with $1+\beta$. In this limit the plasma behaves like a column of noninteracting particles. (2) The cut-off radius r_c depends only weakly on T and β so long as $\lambda_d < r_p$ and β is not too large. However, it moves outwards as $\lambda_d \to r_p$.

Except when $\lambda_{dL} \ll r_p$, the density does not quite increase proportional to the magnetic field. Consequently, the $\mathbf{E}\times\mathbf{B}$ self-rotation frequency of the plasma is not constant along field lines. However, it is easy to prove (see Appendix B) that the total rotation frequency, the sum of the $\mathbf{E}\times\mathbf{B}$ rotation frequency and the diamagnetic drift rotation frequency, is constant along field lines.

Nothing presented in this paper requires that the rotation frequency be the same on all field lines and at all radii. If it is, the plasma is in the more restricted state of global thermal equilibrium. Formally,[4] the global equilibrium density distribution function is proportional to $\exp[-(H-wp_\theta)/kT]$, where H is the electron energy and p_θ is canonical angular momentum. The rotation frequency ω is everywhere constant. Typically, global equilibrium is attained via transport across field lines, and if attained at all, occurs long after local equilibrium along field lines is achieved. It is easy enough to find global equilibrium states in mirror fields, but as no new physics occurs, global equilibrium will not be explored further.

III. SEPARATRICES AND TRAPPING

It is well known that increasing magnetic fields repel electrons with high perpendicular velocities. From conservation of magnetic moment and energy, it is easy to derive a

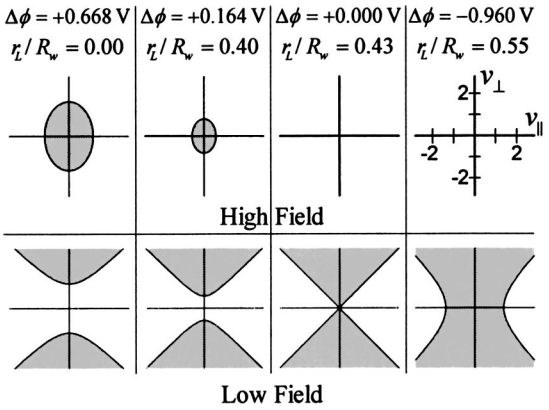

FIG. 6. The separatrices between trapped (shaded) and untrapped noninteracting particles for $\beta=1$. The parallel $v_\parallel$ and perpendicular temperatures $v_\perp$ are normalized to the thermal temperature. The scale used in all the graphs is identical to the scale in the upper right graph. The density profile and potential are identical to those shown in Fig. 4. The appropriate separatrices are plotted at the four indicated potentials, corresponding to the indicated low field radii. There are no trapped particles in the high field region for $r_L/R_w > 0.43$ because there $\Delta\phi \leqslant 0$.

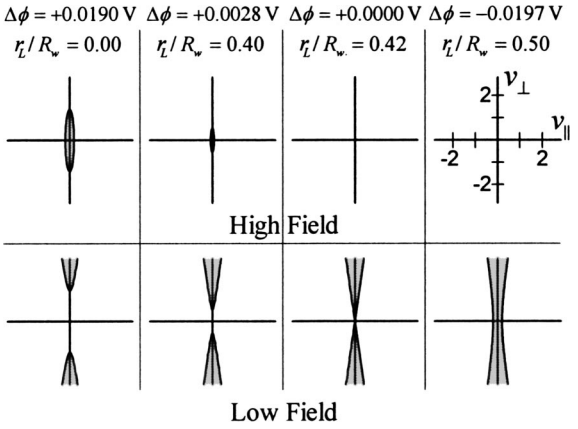

FIG. 7. The separatrices between trapped (shaded) and untrapped noninteracting particles for $\beta=0.02$. Other parameters are identical to those in Fig. 6. Note that the separatrices in this figure resemble those in Fig. 6 if the $v_\parallel$ axis is normalized by $\sqrt{\beta}$.

separatrix between particles which are reflected by the increasing field and particles which can penetrate into the higher fields

$$v_{\perp sL}(v_\parallel) = \sqrt{\frac{1}{\beta}\left(v_\parallel^2 + \frac{2e\Delta\phi}{kT}\right)}, \tag{4}$$

where the velocities have been normalized by the thermal velocity $v_T = \sqrt{kT/m}$. Thus, for a given $v_\parallel$, particles with *larger* perpendicular velocities than $v_{\perp sL}(v_\parallel)$ will be reflected. When $\Delta\phi$ is zero, the result is well known; the separatrix reduces to the straight lines with slope $\pm\sqrt{1/\beta}$ shown in Fig. 1. Including the $\Delta\phi$ term extends this result to non-neutral plasma equilibria, and changes the form of the separatrix to a hyperbola.

Equation (4) describes the separatrix for particles transiting from the low to the high field region. If $\Delta\phi$ is positive, some particles will be reflected while attempting to transit the other way, from the high to the low field region. The high-field separatrix is defined by

$$v_{\perp sH}(v_\parallel) = \sqrt{\frac{1+\beta}{\beta}\left(\frac{2e\Delta\phi}{kT} - v_\parallel^2\right)}, \tag{5}$$

an ellipse; particles with perpendicular energy *less* than $v_{\perp sH}(v_\parallel)$ will be reflected. As no particles are reflected when $\Delta\phi$ is zero or negative, this separatrix does not exist for non-interacting particles or for neutral plasmas.

Typical examples of both the high and low separatrices are plotted in Figs. 6 and 7. Particles which are reflected will be trapped; thus, separate populations of particles are trapped in both the low and high field regions. The fraction of the population that is trapped in the low field region is slightly less than one can calculate explicitly for the $\Delta\phi=0$ case, namely $\sqrt{\beta/(1+\beta)}$. The fraction trapped in the high field region is typically two to ten times lower.

One might think that the origin of the hyperbolic low-to-high separatrix might go to zero as β goes to zero (at $r=0$); in other words, the separatrix might asymptote to the classic form shown in Fig. 1. Likewise, the high-to-low separatrix might disappear entirely. However, Eqs. (2) and (3), as well as the numeric solutions, predict that $e\Delta\phi(0)/kT \to \beta$ as $\beta \to 0$ and $r_p \gg \lambda_d$. Consequently, the value of the perpendicular velocity on the separatrix at $v_\parallel = 0$ $[v_{\perp s}(0;r=0)]$ is never far from the thermal velocity. Significant differences between the correct form of the separatrix and the classic form $(\Delta\phi=0)$ persist up to normalized velocities in the vicinity of $\sqrt{2\beta}$.

The qualitative form of the potential difference $\Delta\phi(r)$ is a displaced exponential; $e\Delta\phi(r)/kT$ remains close to β until r approaches the edge of the plasma [see Fig. 4(c)]. Thus, the inclusion of the potential $\Delta\phi$ makes a zeroth-order change to the separatrix for almost all the particles; the effects of $\Delta\phi$ do not go away as β vanishes. Only when $r_p \lesssim \lambda_d$ will $e\Delta\phi(0)/kT$ go to zero and $v_{\perp s}(0;r=0)$ approach zero.

IV. SEPARATRIX CROSSING AND TRAPPED PARTICLE MODES

Recent experiments have probed[2] the separatrix. The experiments examined the damping of trapped particle modes: Diocotron-like modes which rely on populations of trapped particles that cannot travel the length of the plasma.[10] These modes are damped by velocity-space collisions which transport particles across the trapping separatrix. There is strong experimental evidence that the damping of these modes is closely linked to the hitherto unknown mechanism for global transport in non-neutral plasmas.[1] The damping[11] should be proportional to the value of the distribution function on the separatrix, $f(v_\parallel, v_\perp) = f[v_\parallel, v_{\perp s}(v_\parallel)] = f_s(v_\parallel)$ where $v_{\perp s}$ is found from Eq. (4). Thus, the damping rate should depend on shape of the separatrix.

The damping can be enhanced by an applied rf drive of frequency f_{rf}. The drive kicks particles with a velocity proportional to f_{rf}. (The drive acts over an interaction length L^*, so particles with velocity $v_\parallel \approx L^* f_{\mathrm{rf}}$ will receive a nonadiabatic kick in $v_\parallel$.) The shape of the separatrix can be probed by varying the drive frequency f_{rf}. The authors of Ref. 1 do not consider the true mirror equilibrium, so they

ignore all effects of $\Delta\phi \neq 0$. Assuming a Maxwellian distribution, that β is small, and that $\Delta\phi=0$, they find the following expression for the distribution function on the separatrix [Eq. (5) of Ref. 2]:

$$f_s(v_\parallel) \propto \frac{v_\parallel}{\sqrt{\beta}} \exp\left(-\frac{v_\parallel^2}{2\beta} \right). \tag{6}$$

As the authors find excellent experimental agreement with this formula, they would indeed be tracing out the separatrix straightforwardly if $\Delta\phi$ were zero. (Note that they also assume that the number of kicked particles is independent of v, an assumption quite unresolved by the experiments.)

A proper calculation of $f_s(v_\parallel)$ includes both the directionality of the kick (along $v_\parallel$) and the effects of $\Delta\phi$. The complete formula is

$$\begin{array}{ll} \dfrac{v_\parallel}{\beta} \exp\left(-\dfrac{e\Delta\phi}{\beta kT} \right) \exp\left[-\dfrac{v_\parallel^2}{2}\left(\dfrac{1+\beta}{\beta} \right) \right] & v_\parallel^2 > -\dfrac{2e\Delta\phi}{kT} \\ 0 & v_\parallel^2 \leqslant -\dfrac{2e\Delta\phi}{kT}. \end{array} \tag{7}$$

Curiously, this equation is proportional to Eq. (6) in the limit $\beta \to 0$ and when the velocity cutoff $v_\parallel^2 > -2e\Delta\phi/kT$ is satisfied. Equation (7) should be weighted over the currently unknown mode profile; since the bulk of the plasma satisfies the velocity cutoff, Eq. (6) and Eq. (7) likely predict similar damping. Thus, the experiments in Ref. 1 cannot differentiate between the separatrix solutions found in this paper and the standard separatrix ($\Delta\phi=0$).

Note, however, that the velocity cutoff is violated for large radii where $\Delta\phi<0$. Assuming uniform weighting, there are small differences between the two equations that are comparable to the resolution of the experiments. If the mode was concentrated at the very edge of the plasma, however, there would be significant differences between the equations. Thus, the experiments imply that the mode extends throughout the bulk.

The proportionality between Eqs. (6) and (7) is, in some sense, coincidental. For instance, for kicks along $v_\perp$ instead of $v_\parallel$, the $\Delta\phi=0$ solution resembles the proper solution only when v is much larger than the thermal velocity. Likewise, the mode should also be damped by crossings of the high field separatrix. The form of $f_s(v_\parallel)$ on the high field separatrix is completely different from Eqs. (6) and (7), as it is zero beyond a cut-off velocity comparable to $v_T/\sqrt{\beta}$. Finally, the natural mode damping from collisions is strongly dependant on the nature of the separatrix and will not reduce to the $\Delta\phi=0$ limit.

V. CONCLUSIONS

Because the potential is not constant along field lines, mirror non-neutral plasma equilibria are quite different from noninteracting particle equilibria or uniform field non-neutral equilibria. Separate populations of particles are trapped in both the high and low field regions. The trapped populations exist throughout the plasma, not just at the radial edge. There is a qualitative change in the form of the separatrices dividing trapped and untrapped particles from the commonly described mirror separatrix. The unusual nature of the separatrices complicates the interpretation of experiments intended to explore these separatrices.

ACKNOWLEDGMENTS

Dr. Ramesh Gopalan aided the development of many of these ideas. I thank Dr. Driscoll, Dr. Dubin, Dr. Kabantsev, Dr. O'Neil, and Dr. Wurtele for their helpful comments.

This work was supported by the Office of Naval Research.

APPENDIX A: FLAT-TOP, SMALL GRADIENT EQUILIBRIA

The equilibrium for a flat-top, finite temperature plasma, in a small mirror field $\beta \gtrsim 0$, can be derived from Poisson's and Boltzmann's equations. As β is small, the density variations are small, and Boltzmann's relation for the density in the low and high field region [Eq. (1)] can be approximated as

$$\begin{aligned} n_L(r_L) &= \mathcal{N}\left(1 - \frac{e\Delta\phi(r_L)}{kT} + \cdots \right), \\ n_H(r_H) &= \mathcal{N}\left(1 + \frac{e\Delta\phi(r_L)}{kT} + \cdots \right), \end{aligned} \tag{A1}$$

where $\mathcal{N}$ is the density when $\beta=0$. From the zero temperature limit discussed in Sec. II A, we know that the density increase between the two limits is approximately β. Thus, a good starting approximation for the potential difference along a field line is

$$\Delta\phi(r_L) = \frac{kT\beta}{e}[1 - \Delta\varphi_L(r_L)], \tag{A2}$$

where $\Delta\varphi_L(r_L \approx 0)$ is small when $r_{pL} \gg \lambda_D$.

Recall that the potential difference along a field line is defined by

$$\Delta\phi(r_L) = \Phi_H(r_H) - \Phi_L(r_L), \tag{A3}$$

where $\Phi_L(r_L)$ and $\Phi_H(r_H)$ are the potentials in the low and high field regions as a function of radius, and where, as usual, r_L and r_H are linked by a field line. Assuming the plasma in the low field region resembles a long charge rod, Poisson's equation can be trivially integrated to give

$$\begin{aligned} \Phi_L(r_L) = &\frac{e}{\epsilon_0} \int_{r_{pL}}^{r_L} \frac{dr}{r} \int_0^r d\tilde{r}\, \tilde{r} n_L(\tilde{r}) \\ &+ \frac{e}{\epsilon_0} \ln\left(\frac{r_{pL}}{R_w} \right) \int_0^{r_{pL}} dr\, r n_L(r). \end{aligned} \tag{A4}$$

Using Eqs. (A1) and (A2) reduces this equation to

$$\Phi_L(r_L)=\frac{e\mathcal{N}}{\epsilon_0}\left\{(1-\beta/2)\left[\frac{1}{4}(r_L^2-r_{pL}^2)+\frac{1}{2}r_{pL}^2\ln\left(\frac{r_{pL}}{R_w}\right)\right]+\frac{\beta}{2}\left[\int_{r_{pL}}^{r_L}\frac{dr}{r}\int_0^r d\tilde{r}\,\tilde{r}\Delta\varphi_L(\tilde{r})+\ln\left(\frac{r_{pL}}{R_w}\right)\int_0^{r_{pL}}dr\,r\Delta\varphi_L(r)\right]\right\}. \tag{A5}$$

Similarly

$$\Phi_H(r_H)=\frac{e\mathcal{N}}{\epsilon_0}\left\{(1+\beta/2)\left[\frac{1}{4}(r_H^2-r_{pH}^2)+\frac{1}{2}r_{pH}^2\ln\left(\frac{r_{pH}}{R_w}\right)\right]-\frac{\beta}{2}\left[\int_{r_{pH}}^{r_H}\frac{dr}{r}\int_0^r d\tilde{r}\,\tilde{r}\Delta\varphi_H(\tilde{r})+\ln\left(\frac{r_{pH}}{R_w}\right)\int_0^{r_{pH}}dr\,r\Delta\varphi_H(\tilde{r})\right]\right\}, \tag{A6}$$

where $\Delta\varphi_H(r)$ equals $\Delta\varphi_L(r)$ at linked radii. With the aid of the identities

$$\int_0^{r_{pH}}dr\,r\Delta\varphi_H(r)=(1-\beta)\int_0^{r_{pL}}dr\,r\Delta\varphi_L(r) \tag{A7}$$

and

$$\int_{r_{pH}}^{r_H}\frac{dr}{r}\int_0^r d\tilde{r}\,\tilde{r}\Delta\varphi_H(\tilde{r})=(1-\beta)\int_{r_{pL}}^{r_L}\frac{dr}{r}\int_0^r d\tilde{r}\,\tilde{r}\Delta\varphi_L(\tilde{r}), \tag{A8}$$

substituting Eqs. (A2), (A5), and (A6) into Eq. (A3), and keeping only terms linear in β, gives an integral equation for $\Delta\varphi_L(r)$

$$\frac{kT}{e}[1-\Delta\varphi_L(r_L)]=-\frac{e\mathcal{N}}{\epsilon_0}\left[\frac{r_{pL}^2}{4}+\int_{r_{pL}}^{r_L}\frac{dr}{r}\int_0^r d\tilde{r}\,\tilde{r}\Delta\varphi_L(\tilde{r})+\ln\left(\frac{r_{pL}}{R_w}\right)\int_0^{r_{pL}}dr\,r\Delta\varphi_L(r)\right]. \tag{A9}$$

Defining $\lambda_d^2=\epsilon_0 kT/\mathcal{N}e^2$, and differentiating this equation twice yields the differential equation for zeroth-order modified Bessel functions

$$0=\rho\frac{d^2\Delta\varphi_L(\rho)}{d\rho^2}+\frac{d\Delta\varphi_L(\rho)}{d\rho}-\rho\Delta\varphi_L(\rho), \tag{A10}$$

where $\rho=r_L/\lambda_d$. Discarding the K_0 solution because its behavior at the origin is not analytic leaves the solution $\Delta\varphi_L(\rho)=AI_0(\rho)$. As Eqs. (A5) and (A6) are only valid inside the plasma, this solution is only valid there as well.

Finally, the coefficient A is found by substituting the solution $AI_0(r_L/\lambda_d)$ into Eq. (A9), and evaluating the resulting equation at $r_L=0$. Employing the identities

$$\int^r d\tilde{r}\,\tilde{r}I_0(\tilde{r}/\lambda_d)=\lambda_d r I_1(r/\lambda_d) \tag{A11}$$

and

$$\int_{r_{pL}}^0\frac{dr}{r}\int_0^r d\tilde{r}\,\tilde{r}I_0(\tilde{r}/\lambda_d)=\lambda_d^2[1-I_0(r_{pL}/\lambda_d)], \tag{A12}$$

yields a linear equation for A which is solved by Eq. (3).

APPENDIX B: ROTATION RATE

So long as the plasma is in local thermal equilibrium, the total rotation frequency will be constant along field lines. The total rotation frequency is the sum of the $\mathbf{E}\times\mathbf{B}$ rotation frequency, E/rB, and the diamagnetic drift rotation frequency $(kT/eBr)d\ln n/dr$. Equating the rotation frequency in the low and high fields gives

$$\frac{1}{r_L}\frac{E_L(r_L)}{B_L}+\frac{1}{r_L}\frac{kT}{eB_L}\frac{d\ln n_L(r_L)}{dr_L}=\frac{1}{r_H}\frac{E_H(r_H)}{B_H}+\frac{1}{r_H}\frac{kT}{eB_H}\frac{d\ln n_H(r_H)}{dr_H}, \tag{B1}$$

where $E_L(r_L)$ and $E_H(r_H)$ are the electric fields in the low and high field regions. Using $B_H=(1+\beta)B_L$, $r_H=r_L/\sqrt{1+\beta}$, and Boltzmann's relation [Eq. (1)] this equation becomes

$$E_L(r_L)-\frac{E_H(r_H)}{\sqrt{1+\beta}}=\frac{kT}{e}\frac{d}{dr_L}\left\{\ln\left[n_L(r_L)\exp\left(\frac{e\Delta\phi(r_L)}{kT}\right)\right]-\ln[n_L(r_L)]\right\}, \tag{B2}$$

or

$$E_L(r_L)-\frac{E_H(r_H)}{\sqrt{1+\beta}}=\frac{d\Delta\phi(r_L)}{dr_L}. \tag{B3}$$

But this is equivalent to the definition of $\Delta\phi$, as can be seen by differentiating Eq. (A3). Thus, the total rotation rate is constant along field lines in local thermal equilibrium.

[1] A. Kabantsev and C. Driscoll, Phys. Rev. Lett. **89**, 245001 (2002).
[2] A. Kabantsev and C. F. Driscoll, Rev. Sci. Instrum. **74**, 1925 (2003).
[3] T. O'Neil and C. Driscoll, Phys. Fluids **22**, 266 (1979).
[4] S. A. Prasad and T. M. O'Neil, Phys. Fluids **22**, 278 (1979).
[5] R. C. Davidson, A. Drobot, and C. A. Kapetanakos, Phys. Fluids **16**, 2199 (1973).
[6] D. Dubin and T. O'Neil, Rev. Mod. Phys. **71**, 87 (1999).
[7] R. Gopalan and J. Fajans, Bull. Am. Phys. Soc. **42**, 1959 (1997).
[8] R. Gopalan and J. Fajans, Bull. Am. Phys. Soc. **43**, 1804 (1998).
[9] R. Gopalan, Ph.D. thesis, University of California, Berkeley (1998).
[10] A. Kabantsev, C. Driscoll, T. Hilsabeck, T. O'Neil, and J. Yu, Phys. Rev. Lett. **87**, 225002 (2001).
[11] Note that the authors of Ref. 2 cannot measure the damping rate directly, but with very good experimental evidence (Ref. 1), they assert that the damping rate is closely coupled to the observed bulk plasma expansion rate.